

Quasi-Large Hole Polarons in BiVO₄: Implications for Photocatalysis and Solar Energy Conversion

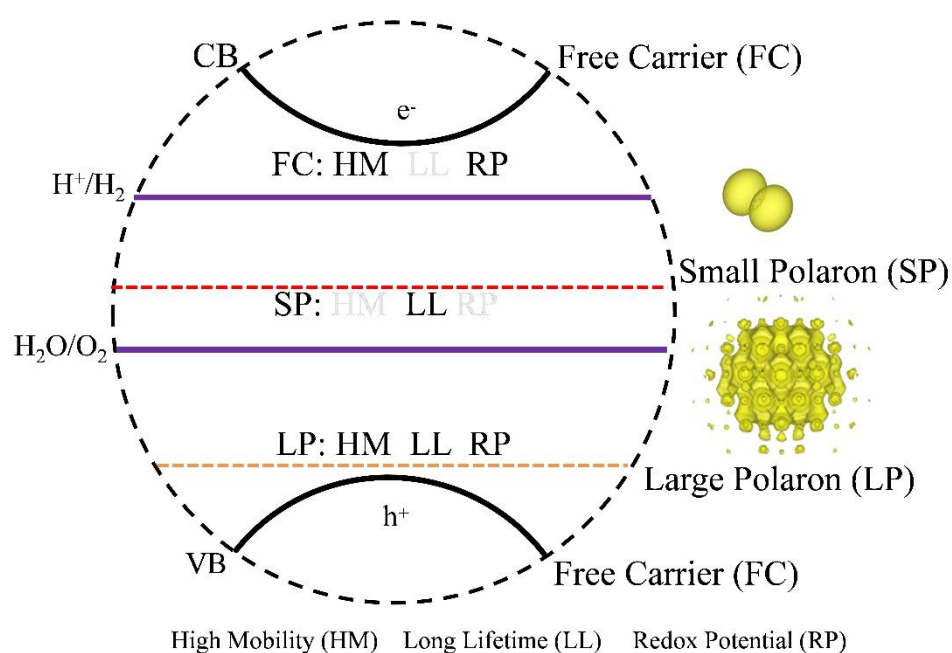
Zhimeng Hao, Taifeng Liu*

National & Local Joint Engineering Research Center for Applied Technology of Hybrid Nanomaterials, Henan University, Kaifeng 475004, China

Corresponding author: Taifeng Liu: tliu@vip.henu.edu.cn

Abstract: BiVO₄ is a promising photocatalyst for solar energy conversion, but its efficiency is limited by small polaron formation. However, some physical properties of BiVO₄ deviate from typical small polaron behavior. Using the state-of-the-art first-principles calculations, we demonstrate that BiVO₄ forms a quasi-large hole polaron with a radius around 2 nm, resembling free carriers with high mobility. This polaron is stabilized primarily by acoustic phonon modes, creating a shallow trap state near the valence band maximum, which prolongs its lifetime. Simultaneously, it retains a redox potential comparable to that of free carriers. We propose that such large polarons explain the superior properties of BiVO₄ and other transition metal oxide photocatalysts. Tuning phonon modes to stabilize large polarons offers a promising strategy for designing materials with enhanced solar energy conversion efficiency.

TOC Graphic



Bismuth vanadate (BiVO_4) has gained significant attention as a photocatalyst and photoelectrochemical material for water splitting, enabling efficient solar-to-chemical energy conversion¹⁻⁵. Its advantages include abundant and inexpensive elements⁶, a suitable bandgap for light absorption⁷, and favorable band edges for water oxidation⁸⁻¹⁰. Key factors affecting solar energy conversion efficiency—such as charge carrier mobility, lifetime, and diffusion length—determine charge separation and transport^{11, 12}. Time-resolved microwave conductivity (TRMC) experiments report a carrier mobility of $0.04 \text{ cm}^2 \text{ V}^{-1} \text{ s}^{-1}$, a lifetime of 40 ns, and a diffusion length of 70 nm in BiVO_4 ¹³, contributing to its excellent solar energy conversion performance. These properties are strongly mediated by polaron formation, a phenomenon prevalent in BiVO_4 and other transition metal oxides¹⁴.

Both electron and hole polarons in BiVO_4 have been extensively studied through theoretical and experimental approaches. For electrons, density functional theory (DFT) with on-site Coulomb corrections (DFT+U) and hybrid DFT methods consistently show electron localization on vanadium atoms, forming small polarons^{15, 16}. This self-trapping induces significant local lattice distortions, reducing V^{5+} to V^{4+} .¹⁷ The small polaron exhibits an activation energy of $\sim 0.35 \text{ eV}$ for nearest-neighbor hopping, with mobility on the order of $10^{-4} \text{ cm}^2 \text{ V}^{-1} \text{ s}^{-1}$ ^{18, 19}. This localization creates a deep trap state approximately 1 eV below the conduction band minimum (CBM).

For hole carriers in BiVO_4 , localization differs across computational approaches. Using DFT+U, the hole self-traps on a single oxygen atom, forming a small hole polaron with significant lattice distortion and a charge transition from O^{2-} to O^- . In contrast, hybrid functionals predict a hole localized on the BiO_8 dodecahedron, with $\sim 20\%$ of the charge on the Bi atom, characterized by Bi 6s orbitals^{20, 21}. Both types are classified as small polarons, forming deep trap states ($\sim 1 \text{ eV}$ above the valence band maximum, VBM) primarily from O 2p or hybridized Bi 6s orbitals^{16, 22}. The small hole polaron has an activation energy of $\sim 0.3 \text{ eV}$ for hopping and a mobility on the order of $10^{-4} \text{ cm}^2 \text{ V}^{-1} \text{ s}^{-1}$ ²³. Recent several studies have revealed that holes in BiVO_4 exhibit a more delocalized state compared to electrons. Sun et al.²⁴ employed pump-probe transient reflection microscopy to directly observe electron and hole dynamics in BiVO_4 . Their findings reveal that electrons are more localized, while holes exhibit greater delocalization. Seo et al.²⁵ investigated the hole polaron in BiVO_4 using hybrid DFT with a $4 \times 4 \times 2$ supercell (768 atoms). They revealed that the self-trapped energy of hole polaron is -0.1 eV which may result in free carriers in the valence band (VB).

Additionally, their study found that with smaller supercells ($3 \times 3 \times 1$ and $3 \times 3 \times 2$), holes do not localize.

Current research suggests small polaron formation in BiVO_4 . However, this model is inconsistent with experimental measurements²⁴, as small polaron hopping predicts much lower mobility. Furthermore, deep trap states associated with small polarons impair water oxidation performance. The conclusions of small polaron formation heavily depend on computational parameters such as the U value in DFT+ U or the Hartree-Fock exchange fraction (α) in hybrid functionals.

In this study, we investigated polarons in BiVO_4 without employing the supercell approach, eliminating the need for DFT+ U or hybrid functionals. we employ a state-of-the-art first-principles approach accounting for electron-phonon coupling to investigate polarons in BiVO_4 . The ab initio polaron equations were solved to accurately model isolated polarons¹⁶. We identify a quasi-large hole polaron which could explain the experimental findings. This polaron forms a shallow trap state, enhancing its lifetime without compromising water oxidation capability.

The ground state wave function $\psi(r)$ and atomic displacements $\Delta\tau_{k\alpha p}$ forming a polaron can be found by minimizing the total DFT energy functional of an excess electron added to a crystal, which translates into the solution of the following coupled system of equations²⁶,

$$\hat{H}_{KS}^0 \psi(r) + \sum_{k\alpha p} \frac{\partial V_{KS}^0}{\partial \tau_{k\alpha p}} \Delta\tau_{k\alpha p} \psi(r) = \varepsilon \psi(r) \quad (1)$$

$$\Delta\tau_{k\alpha p} = - \sum_{\kappa' \alpha' p'} (C^0)^{-1}_{k\alpha p, \kappa' \alpha' p'} \int dr \frac{\partial V_{KS}^0}{\partial \tau_{\kappa' \alpha' p'}} |\psi(r)|^2 \quad (2)$$

$\tau_{k\alpha p}$ represents the Cartesian coordinate of the atom k in the unit cell p along the direction α , $C^0_{k\alpha p, \kappa' \alpha' p'}$ is the matrix of interatomic force constants²⁷, and \hat{H}_{KS}^0 and V_{KS}^0 represent the Kohn-Sham Hamiltonian and the self-consistent potential, respectively. The superscript ⁰ indicates that the quantities are evaluated in the ground state without extra electron. We will refer to ε as the polaron eigenvalue²⁸.

We can transform Eqs. (1) and (2) into a coupled set of equations for the expansion coefficients in reciprocal space,

$$\frac{2}{N_p} \sum_{qmv} B_{qv} g_{mnv}^*(K, q) A_{mk+q} = (\varepsilon_{nk} - \varepsilon) A_{nk} \quad (3)$$

$$B_{qv} = \frac{1}{N_p} \sum_{mnk} A_{mk+q}^* \frac{g_{mnv}(k, q)}{\hbar \omega_{qv}} A_{nk} \quad (4)$$

In these expressions, ε_{nk} are the Kohn-Sham eigenvalues, ω_{qv} are the phonon frequencies and $g_{mnv}(K, q)$ are the electron-phonon matrix elements^{29, 30}.

The polaron formation energy ΔE_f , defined as the energy required to trap a conduction band state with eigenvalue ε_{CBM} into a localized polaron. It consists of electron part and phonon part, can be obtained from the expansion coefficients that solve Eqs. (3) and (4) by²⁶:

$$\Delta E_f = \frac{1}{N_p} \sum_{nK} |A_{nK}|^2 (\varepsilon_{nK} - \varepsilon_{CBM}) - \frac{1}{N_p} \sum_{qv} |B_{qv}|^2 \hbar \omega_{qv} \quad (5)$$

ε_{CBM} are the kohn-Sham eigenvalue of the conduction band bottom, \hbar are the reduced Plank constant. ε_{nk} are the Kohn-Sham eigenvalues, ω_{qv} are the phonon frequencies. A_{nk} is the coefficient of the single-particle Kohn-Sham state used to expand the polaron wave function, and B_{qv} is the coefficient of phonon eigenmodes with frequencies ω_{qv} to expand the atomic displacement²⁶.

We performed density functional theory (DFT) calculations using the Quantum ESPRESSO package³¹⁻³³ along with Wannier90³³⁻³⁵ and EPW codes^{29, 30, 36}. Calculations were based on the Perdew-Burke-Ernzerh (PBE) parameterization of the exchange-correlation potential within the generalized gradient approximation (GGA)^{32, 33}, using optimized norm-conserving Vanderbilt (ONCV) pseudopotentials and plane waves with a kinetic energy cutoff of 90 Ry³⁷⁻³⁹. Phonon frequencies and electron-phonon matrix elements were determined through density functional perturbation theory. Ground state electron and lattice dynamics were calculated using $4 \times 4 \times 8$ k-point and $2 \times 2 \times 4$ q-point grids, respectively. The electron energies, phonon frequencies, and electron-phonon matrix elements interpolated onto dense grids through Wannier-Fourier interpolation with $8 \times 8 \times 8$ k-points and $8 \times 8 \times 8$ q-points. To obtain maximally localized Wannier functions, we included a subset comprising

the 10 lowest conduction bands investigating electron polarons, 2 and 24 highest valence bands investigate hole polarons on bismuth and oxygen sites, respectively. We calculate the formation of polarons using an $8 \times 8 \times 8$ primitive cell containing 6144 atoms to ensure that the periodic replicas of the polaron are sufficiently separated.

We systematically investigated all types of polarons, including hole and electron polarons, in tetragonal BiVO_4 using first-principles calculations. It is modeled using a 12-atom primitive cell for both geometry optimization and phonon calculations. The calculated lattice parameters, $a = b = c = 6.93 \text{ \AA}$, $\alpha = \beta = 136.19^\circ$, $\gamma = 63.69^\circ$, agree well with experimental values⁴⁰. For a hole polaron, localization can occur either at oxygen or bismuth sites, and both scenarios were investigated in our study. We first investigated the hole localized on the oxygen sites. The isosurface plot of the polaron wavefunction for a hole localized on oxygen sites is shown in Figure 1(a). Unlike DFT+U or hybrid functional results¹⁶, which predict localization on a single oxygen site, our calculations reveal the hole is distributed mainly across eight oxygen sites with O 2p character. The polaron radius is around 2 nm, larger than the lattice parameters of a BiVO_4 unit cell. The hole polaron has a formation energy of -22 meV, indicating stability, and forms a shallow trap state 0.18 eV above the valence band maximum (VBM).

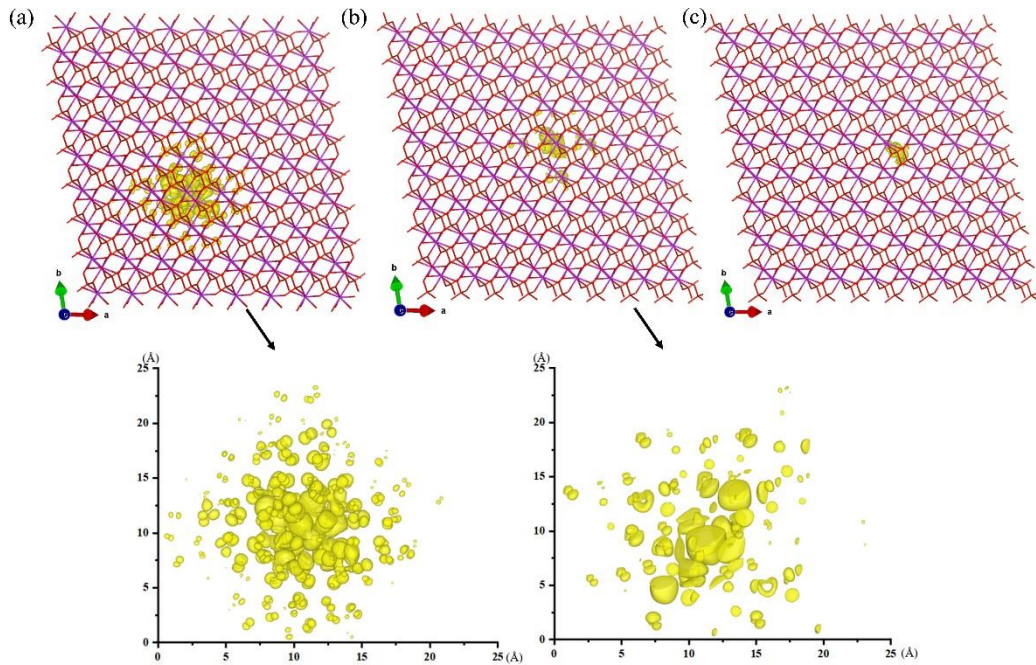


Figure 1 The isosurface plot of the hole polaron wavefunction on (a) O and (b) Bi sites with the insert figures to enlarge the polaron shape, and (c) the isosurface plot of the electron polaron wavefunction on V site

For the hole polaron on bismuth, the hole is primarily localized on two Bi atoms, with the remainder distributed across surrounding oxygen atoms, as shown in the isosurface plot of the polaron wavefunction in Figure 1(b). On Bi atoms, the hole occupies Bi 6s states, while on oxygen atoms, it resides in O 2p states. This result differs from hybrid functional calculations⁴¹, which predict localization on a BiO₈ dodecahedron. Our findings indicate a more delocalized hole polaron, with a radius exceeding 2 nm, including the size of the contribution on oxygen sites. The formation energy of this polaron is -62 meV, making it more stable than the hole polaron on oxygen sites. The trap state is 0.32 eV above the valence band maximum (VBM), slightly deeper than that of the oxygen-site hole polaron.

We identified two types of hole polarons in BiVO₄, both with radii exceeding the unit cell lattice parameters. Compared to large polarons in materials like LiF⁴² or halide perovskites⁴³, which have radius larger than 3 nm, the hole polaron in BiVO₄ is classified as a quasi-large polaron. With a radius between that of small and large polarons, its transport can involve hopping or free-carrier behavior, yielding mobility exceeding 1 cm²V⁻¹s⁻¹.

For electron carriers, a small polaron forms, localized on a vanadium site as shown in Figure 1(c). This result aligns with findings from both DFT+U and hybrid functional approaches, which consistently indicate that the electron forms a small polaron localized on the vanadium site. The radius of this small polaron is approximately 0.5 nm. This small polaron has a formation energy of -501 meV, significantly lower than that of the hole polaron, reflecting stronger localization. The trap state lies 1.43 eV below the CBM, deep within the 2.46 eV band gap, confirming its deep-trap nature. The activation energy for hopping is ~0.35 eV, with mobility in the 10⁻⁴ cm²V⁻¹s⁻¹ range^{18, 19}.

We investigated electron and hole polarons in BiVO₄ from the perspective of electron-phonon coupling. For hole polarons localized on oxygen sites, the electronic weights $|A_{nk}|^2$ superimposed on the band structure and the spectral function $A^2(E)$ are shown in Figure 2(a), while the corresponding atomic displacements resolved by $|B_{qv}|^2$ and the phonon spectral function $B^2(E)$ are shown in Figure 2(b). Similarly, the electron and phonon contributions for hole polarons localized on bismuth sites are displayed in Figures 2(c) and 2(d).

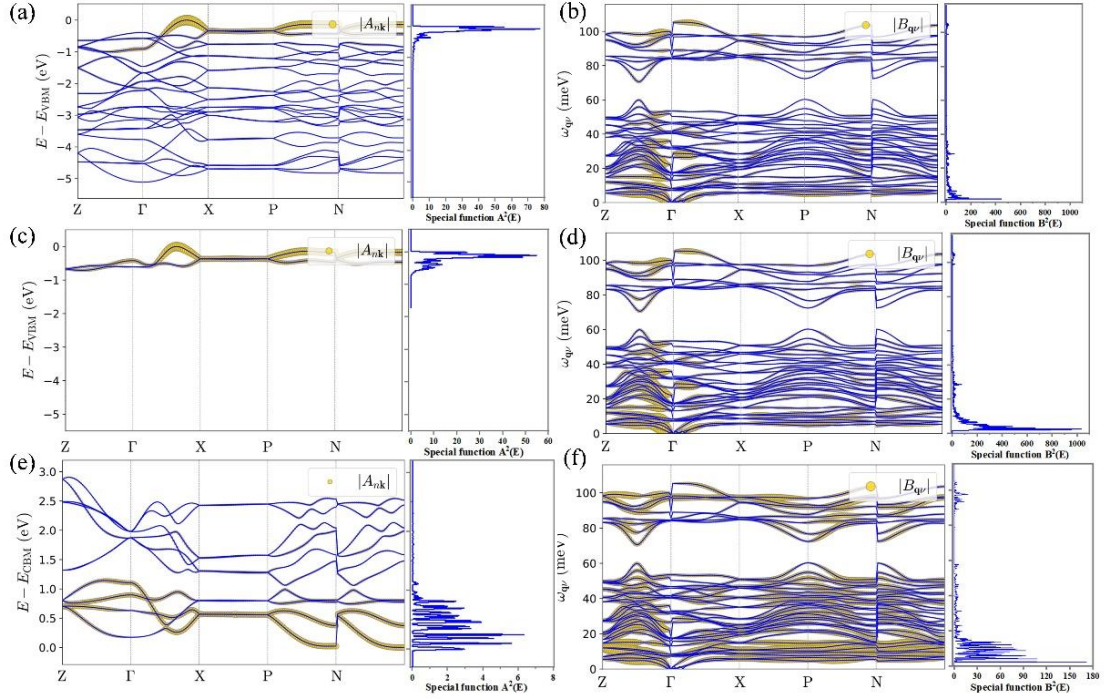


Figure 2 Generalized Fourier amplitudes A_{nk} plotted on top of the phonon dispersion relations of BiVO_4 and spectral function $A^2(E)$. Generalized Fourier amplitudes B_{qv} plotted on top of the phonon dispersion relations of BiVO_4 and spectral function $B^2(E)$. The hole polaron localization on (a) and (b) O sites, (c) and (d) Bi sites. (e) and (f) The electron polaron localization on V sites. The corresponding points of transverse wave vector k are Z(0.5, 0.5, -0.5), G(0.0, 0.0, 0.0), X(0.0, 0.0, 0.5), P(0.25, 0.25, 0.25), N(0.0, 0.5, 0.0).

Hole polarons are primarily associated with states at the top of the valence band, with minimal contributions from deeper valence band states. Phonon spectra reveal that transverse acoustic modes (<10 meV) dominate the coupling, with minor contributions from longitudinal optical (LO) modes at ~ 50 and ~ 100 meV. For oxygen-site hole polarons, phonon contributions amount to -0.16 eV, while electron contributions are 0.14 eV. For bismuth-site hole polarons, the respective contributions are -0.26 eV and 0.20 eV, explaining the greater stability of bismuth-site polarons. Notably, phonon energies forming bismuth-site polarons are nearly double those forming oxygen-site polarons.

For electron polarons localized on vanadium sites, Figures 2(e) and 2(f) show the electron and phonon contributions. The entire lowest conduction band contributes significantly to the polaronic wavefunction, with smaller contributions from higher bands. Coupling involves the entire LO phonon branch, with dominant contributions from modes below 20 meV and additional contributions from modes in the 80 – 100 meV range. The total phonon contribution is -0.87 eV, while the electron contribution is 0.42 eV, indicating strong

electron-phonon coupling and small polaron formation for electrons. In contrast, the weaker electron-phonon coupling for holes leads to quasi-large polaron formation. These findings highlight distinct coupling mechanisms for electron and hole polarons in BiVO₄, with implications for charge transport and material performance.

Several experimental measurements are available for comparison with our calculated results. Early studies using TMRC¹³ and THz⁴⁴ spectroscopy reported carrier mobilities on the order of $10^{-2} \text{ cm}^2 \text{ V}^{-1} \text{ s}^{-1}$, but these methods cannot distinguish between electrons and holes. Experimental mobility values are expected to be lower than theoretical predictions due to sample impurities and surface boundary effects, as our calculations assume a perfect crystal. Chi et al.⁴⁵ predicted the existence of large hole polarons in BiVO₄, attributed to O p orbitals hybridized with V and Bi sp orbitals. Additionally, our calculated results demonstrate that holes form quasi-large polarons, directly supporting the findings of Sun et al.²⁴ and Seo et al.²⁵, which indicate that holes exhibit greater delocalization.

When the photocatalyst BiVO₄ absorbs photons, free carriers (electrons and holes) are generated, as depicted in Figure 3. These carriers exhibit high mobility and have conduction band (CB) and valence band (VB) levels suitable for redox reactions. However, free carriers typically have short lifetimes due to rapid recombination. Fortunately, they can transform into polarons, which act as trapped states with extended lifetimes.

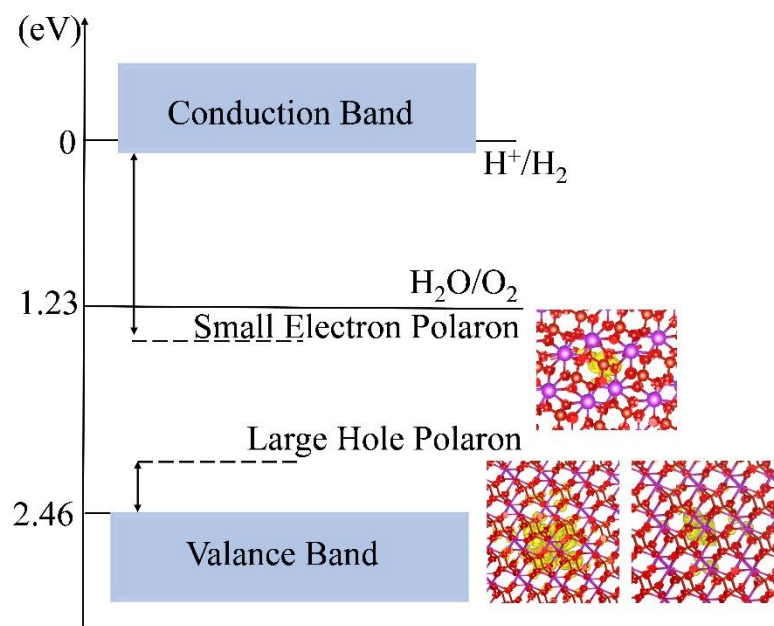


Figure 3 The energy level of the trap states of different types of polarons in the band gap of BiVO₄.

Small polarons are commonly observed in photocatalysts. While their lifetimes are longer, their mobility is extremely low ($10^{-4} \text{ cm}^2 \text{ V}^{-1} \text{ s}^{-1}$). Additionally, small polarons often form deep trap states in the middle of the band gap, which can impair redox activity, as illustrated in Figure 3. Quasi-large or large polarons may also form in photocatalysts, although they remain less explored due to methodological limitations. Recent studies have reported large hole polarons in rutile TiO₂, quasi-2D electron polarons in anatase TiO₂⁴⁶, and potential large polarons in tungsten-based photocatalysts such as WO₃⁴⁷, Bi₂WO₆⁴⁸, and certain oxynitrides and nitrides^{49, 50}. Large polarons exhibit mobility comparable to free carriers and form shallow trap states that minimally affect redox reactions. Most importantly, their trapped states have sufficiently long lifetimes to facilitate surface reactions.

In this study, we have identified a quasi-large hole polaron in BiVO₄. This hole polaron can be localized either on oxygen sites or on two bismuth sites along with the surrounding oxygen atoms. The radius of the polaron exceeds the lattice parameters of the BiVO₄ unit cell. It exhibits high mobility comparable to that of free carriers and forms a very shallow trap state close to the valence band maximum (VBM). The transverse acoustic phonon modes play a significant role in stabilizing this hole polaron. Based on these findings, we propose that quasi-large and large polarons are critical in photocatalysis, not only in BiVO₄ but also in other transition metal oxides. Their high mobility ensures efficient charge transport, while their shallow trap states provide extended lifetimes without compromising the redox capabilities of the material. Moreover, phonon modes significantly influence the formation and characteristics of large polarons. By controlling these phonon modes, it may be possible to tune the polaron radius, mobility, and trap states, paving the way for designing high-efficiency materials for solar energy conversion.

ASSOCIATED CONTENT

Notes

The authors declare no competing financial interest.

Data available

The data that support the findings of this study are available from the corresponding author upon reasonable request.

ACKNOWLEDGMENT

This work was supported the Key Technologies R&D Program of Henan Province (No. 242102521002) and the National Natural Science Foundation of China (grant #22173026, 21703054).

Reference

1. Zhu, J.; Fan, F.; Chen, R.; An, H.; Feng, Z.; Li, C., Direct imaging of highly anisotropic photogenerated charge separations on different facets of a single BiVO₄ photocatalyst. *Angewandte Chemie* **2015**, *127* (31), 9239-9242.
2. Li, R.; Han, H.; Zhang, F.; Wang, D.; Li, C., Highly efficient photocatalysts constructed by rational assembly of dual-cocatalysts separately on different facets of BiVO₄. *Energy & Environmental Science* **2014**, *7* (4), 1369-1376.
3. Li, R.; Zhang, F.; Wang, D.; Yang, J.; Li, M.; Zhu, J.; Zhou, X.; Han, H.; Li, C., Spatial separation of photogenerated electrons and holes among {010} and {110} crystal facets of BiVO₄. *Nature Communications* **2013**, *4* (1), 1432.
4. He, T.; Zhao, Y.; Benetti, D.; Moss, B.; Tian, L.; Selim, S.; Li, R.; Fan, F.; Li, Q.; Wang, X., Facet-Engineered BiVO₄ Photocatalysts for Water Oxidation: Lifetime Gain Versus Energetic Loss. *Journal of the American Chemical Society* **2024**, *146* (39), 27080-27089.
5. Qi, Y.; Zhang, J.; Kong, Y.; Zhao, Y.; Chen, S.; Li, D.; Liu, W.; Chen, Y.; Xie, T.; Cui, J., Unraveling of cocatalysts photodeposited selectively on facets of BiVO₄ to boost solar water splitting. *Nature Communications* **2022**, *13* (1), 484.
6. Talasila, G.; Sachdev, S.; Srivastva, U.; Saxena, D.; Ramakumar, S., Modified synthesis of BiVO₄ and effect of doping (Mo or W) on its photoelectrochemical performance for water splitting. *Energy reports* **2020**, *6*, 1963-1972.
7. Park, Y.; Kang, D.; Choi, K.-S., Marked enhancement in electron-hole separation achieved in the low bias region using electrochemically prepared Mo-doped BiVO₄ photoanodes. *Physical Chemistry Chemical Physics* **2014**, *16* (3), 1238-1246.
8. Walter, M.; Warren, E.L.; McKone, J.M.; Boettcher, S.W.; Mi, Q.; Santori, A.; Lewis, S.N. *Chem. Rev* **2010**, *110*, 6446-6473.
9. Rettie, A. J.; Chemelewski, W. D.; Lindemuth, J.; McCloy, J. S.; Marshall, L. G.; Zhou, J.; Emin, D.; Mullins, C. B., Anisotropic small-polaron hopping in W: BiVO₄ single crystals. *Applied Physics Letters* **2015**, *106* (2).
10. Wiktor, J.; Ambrosio, F.; Pasquarello, A., Role of Polarons in Water Splitting: The Case of BiVO₄. *ACS Energy Lett.* **2018**, *3* (7), 1693-1697.
11. Butler, M.; Ginley, D., Principles of photoelectrochemical, solar energy conversion. *Journal of materials science* **1980**, *15*, 1-19.
12. Li, J.; Wu, N., Semiconductor-based photocatalysts and photoelectrochemical cells for solar fuel generation: a review. *Catalysis Science & Technology* **2015**, *5* (3), 1360-1384.
13. Abdi, F. F.; Savenije, T. J.; May, M. M.; Dam, B.; van de Krol, R., The origin of slow carrier transport in BiVO₄ thin film photoanodes: a time-resolved microwave conductivity study. *J. Phys. Chem. Lett.* **2013**, *4* (16), 2752-2757.
14. Ren, Z.; Shi, Z.; Feng, H.; Xu, Z.; Hao, W., Recent progresses of polarons: fundamentals and roles in photocatalysis and photoelectrocatalysis. *Advanced Science* **2024**, *11* (37), 2305139.

15. Liu, T.; Zhao, Q.; Li, C.; Lyu, Y.; Dupuis, M., Photocatalytic facet selectivity in BiVO₄ nanoparticles: Polaron electronic structure and thermodynamic stability considerations for photocatalysis. *The Journal of Physical Chemistry C* **2019**, *123* (33), 20142-20151.
16. Liu, T.; Zhou, X.; Dupuis, M.; Li, C., The nature of photogenerated charge separation among different crystal facets of BiVO₄ studied by density functional theory. *Physical Chemistry Chemical Physics* **2015**, *17* (36), 23503-23510.
17. Kweon, K. E.; Hwang, G. S.; Kim, J.; Kim, S.; Kim, S., Electron small polarons and their transport in bismuth vanadate: a first principles study. *Phys. Chem. Chem. Phys.* **2015**, *17* (1), 256-260.
18. Sarker, H. P.; Huda, M. N. In *Formation of Small Polaron and Polaronic Charge Transfer within BiVO₄ Photocatalyst*, Electrochemical Society Meeting Abstracts 235, The Electrochemical Society, Inc.: 2019; pp 1962-1962.
19. Wu, F.; Ping, Y., Combining Landau–Zener theory and kinetic Monte Carlo sampling for small polaron mobility of doped BiVO₄ from first-principles. *J. Mater. Chem. A* **2018**, *6* (41), 20025-20036.
20. Liu, T.; Cui, M.; Dupuis, M., Hole polaron transport in bismuth vanadate BiVO₄ from hybrid density functional theory. *The Journal of Physical Chemistry C* **2020**, *124* (42), 23038-23044.
21. Kweon, K. E.; Hwang, G. S., Structural phase-dependent hole localization and transport in bismuth vanadate. *Physical Review B—Condensed Matter and Materials Physics* **2013**, *87* (20), 205202.
22. Kweon, K. E.; Hwang, G. S., Surface structure and hole localization in bismuth vanadate: a first principles study. *Applied Physics Letters* **2013**, *103* (13).
23. Liu, T.; Pasumarthi, V.; LaPorte, C.; Feng, Z.; Li, Q.; Yang, J.; Li, C.; Dupuis, M., Bimodal hole transport in bulk BiVO₄ from computation. *Journal of Materials Chemistry A* **2018**, *6* (8), 3714-3723.
24. Sun, F.; Deng, Y.; Leng, J.; Shi, M.; Li, C.; Jin, S.; Li, R.; Tian, W., Visualizing Ultrafast Photogenerated Electron and Hole Separation in Facet-Engineered Bismuth Vanadate Crystals. *Journal of the American Chemical Society* **2024**, *146* (45), 31106-31113.
25. Seo, D.; Somjit, V.; Wi, D. H.; Galli, G.; Choi, K.-S., p-Type BiVO₄ for Solar O₂ Reduction to H₂O₂. *Journal of the American Chemical Society* **2025**, *147* (4), 3261-3273.
26. Sio, W. H.; Verdi, C.; Poncé, S.; Giustino, F., Ab initio theory of polarons: Formalism and applications. *Physical Review B* **2019**, *99* (23), 235139.
27. Giustino, F., Electron-phonon interactions from first principles. *Reviews of Modern Physics* **2017**, *89* (1), 015003.
28. Giustino, F., *Materials modelling using density functional theory: properties and predictions*. Oxford University Press: 2014.
29. Lee, H.; Poncé, S.; Bushick, K.; Hajinazar, S.; Lafuente-Bartolome, J.; Leveillee, J.; Lian, C.; Lihm, J.-M.; Macheda, F.; Mori, H., Electron–phonon physics from first principles using the EPW code. *npj Computational Materials* **2023**, *9* (1), 156.
30. Poncé, S.; Margine, E. R.; Verdi, C.; Giustino, F., EPW: Electron–phonon coupling, transport and superconducting properties using maximally localized Wannier functions. *Computer Physics Communications* **2016**, *209*, 116-133.
31. Giannozzi, P.; Andreussi, O.; Brumme, T.; Bunau, O.; Nardelli, M. B.; Calandra, M.; Car, R.; Cavazzoni, C.; Ceresoli, D.; Cococcioni, M., Advanced capabilities for materials modelling with Quantum ESPRESSO. *Journal of physics: Condensed matter* **2017**, *29* (46), 465901.
32. Giannozzi, P.; Baroni, S.; Bonini, N.; Calandra, M.; Car, R.; Cavazzoni, C.; Ceresoli, D.; Chiarotti, G. L.; Cococcioni, M.; Dabo, I., QUANTUM ESPRESSO: a modular and open-source software project for quantum simulations of materials. *Journal of physics: Condensed matter* **2009**, *21* (39), 395502.
33. Giannozzi, P.; Baseggio, O.; Bonfà, P.; Brunato, D.; Car, R.; Carnimeo, I.; Cavazzoni, C.; De Gironcoli, S.; Delugas, P.; Ferrari Ruffino, F., Quantum ESPRESSO toward the exascale. *The Journal of chemical physics* **2020**, *152* (15).

34. Mostofi, A. A.; Yates, J. R.; Pizzi, G.; Lee, Y.-S.; Souza, I.; Vanderbilt, D.; Marzari, N., An updated version of wannier90: A tool for obtaining maximally-localised Wannier functions. *Computer Physics Communications* **2014**, *185* (8), 2309-2310.
35. Marzari, N.; Mostofi, A. A.; Yates, J. R.; Souza, I.; Vanderbilt, D., Maximally localized Wannier functions: Theory and applications. *Reviews of Modern Physics* **2012**, *84* (4), 1419-1475.
36. Noffsinger, J.; Giustino, F.; Malone, B. D.; Park, C.-H.; Louie, S. G.; Cohen, M. L., EPW: A program for calculating the electron–phonon coupling using maximally localized Wannier functions. *Computer Physics Communications* **2010**, *181* (12), 2140-2148.
37. Scherpelz, P.; Govoni, M.; Hamada, I.; Galli, G., Implementation and validation of fully relativistic GW calculations: spin–orbit coupling in molecules, nanocrystals, and solids. *Journal of chemical theory and computation* **2016**, *12* (8), 3523-3544.
38. Hamann, D., Erratum: optimized norm-conserving vanderbilt pseudopotentials [Phys. Rev. B *88*, 085117 (2013)]. *Physical Review B* **2017**, *95* (23), 239906.
39. Schlipf, M.; Gygi, F., Optimization algorithm for the generation of ONCV pseudopotentials. *Computer Physics Communications* **2015**, *196*, 36-44.
40. David, W.; Glazer, A.; Hewat, A., The structure and ferroelastic phase transition of BiVO₄. *Phase Transitions: A Multinational Journal* **1979**, *1* (2), 155-169.
41. Wiktor, J.; Pasquarello, A., Electron and Hole Polarons at the BiVO₄–Water Interface. *ACS Applied Materials & Interfaces* **2019**, *11* (20), 18423-18426.
42. Sio, W. H.; Verdi, C.; Poncé, S.; Giustino, F., Ab initio theory of polarons: Formalism and applications. *Physical Review B* **2019**, *99* (23).
43. Lafuente-Bartolome, J.; Lian, C.; Giustino, F., Topological polarons in halide perovskites. *Proceedings of the National Academy of Sciences* **2024**, *121* (21), e2318151121.
44. Ziwrtsch, M.; Müller, S. n.; Hempel, H.; Unold, T.; Abdi, F. F.; van de Krol, R.; Friedrich, D.; Eichberger, R., Direct time-resolved observation of carrier trapping and polaron conductivity in BiVO₄. *ACS Energy Lett.* **2016**, *1* (5), 888-894.
45. Chi, X.; Mandal, L.; Liu, C.; Fauzi, A. D.; Chaudhuri, A.; Whitcher, T. J.; Jani, H. K.; Chen, Z.; Xi, S.; Diao, C.; Naradipa, M. A.; Yu, X.; Yang, P.; Castro-Neto, A. H.; Breese, M. B. H.; Loh, K. P.; Venkatesan, T. V.; Rusydi, A., Unravelling a new many-body large-hole polaron in a transition metal oxide that promotes high photocatalytic activity. *NPG Asia Materials* **2022**, *14* (1).
46. Dai, Z.; Giustino, F., Identification of large polarons and exciton polarons in rutile and anatase polymorphs of titanium dioxide. *Proceedings of the National Academy of Sciences* **2024**, *121* (48), e2414203121.
47. Tao, J.; Liu, T., Electron and Hole Polaron Formation and Transport in Monoclinic WO₃ Studied by Hybrid Functional Approach. *The Journal of Physical Chemistry C* **2023**, *127* (32), 16204-16210.
48. Tao, J.; Zhang, Q.; Liu, T., Polaron formation and transport in Bi₂WO₆ studied by DFT+ U and hybrid PBE0 functional approaches. *Physical Chemistry Chemical Physics* **2022**, *24* (37), 22918-22927.
49. Morbec, J. M.; Galli, G., Charge transport properties of bulk Ta₃N₅ from first principles. *Physical Review B* **2016**, *93* (3), 035201.
50. Zhao, Q.; Cui, M.; Liu, T., Charge Carrier Transport Mechanism in Ta₂O₅, TaON and Ta₃N₅ Studied by Polaron Hopping and Bandlike Models. *arXiv preprint arXiv:2105.03108* **2021**.